NDE2002 predict. assure. improve.
National Seminar of ISNT
Chennai, 5. – 7. 12. 2002
www.nde2002.org

DATA ANALYSIS TECHNIQUES IN THERMOGRAPHIC NDT OF COMPOSITE: A CRITICAL COMPARISON

Sanjith G.Zacharia, J.Lahiri

Directorate of Advanced Composites
Advanced Systems Laboratory
Hyderabad – 500 058
EMAIL: SANJITH@VSNL.COM

DATA ANALYSIS TECHNIQUES IN THERMOGRAPHIC NDT OF COMPOSITE: A CRITICAL COMPARISON

Sanjith G.Zacharia, J.Lahiri

Directorate of Advanced Composites
Advanced Systems Laboratory
Hyderabad – 500 058
email: sanjith@vsnl.com

1.0 INTRODUCTION

Thermography is a relatively new and fast emerging area of inspection methodology in the field of non-destructive testing. This involves the use of an IR camera to capture the evolution of surface temperature profiles of the test object, after being subjected to thermal perturbation from a high energy uniform light source. Inspite of serious drawbacks of poor penetration and low signal-to-noise ratio, the fast, contact-less and couplant-free inspection procedure involved in thermography has much promise in certain applications.

Thermal energy deposition is conventionally carried out in two ways, i.the pulse mode (pulse thermography) wherein the thermal energy is sent out in a burst ii.the standing wave mode (lock-in thermography) where the thermal waves are made to constantly impinge on the specimen. The ease and speed with which pulse thermography can be carried out, has much potential for its practical usage in the shop floor. However, visualizing the pulse as a combination of sinusoids, the specific advantages of lock-in thermography were later integrated into this much simpler technique in the form of 'pulse phase thermography'.

Much effort has been made by different researchers in this field towards developing appropriate data analysis techniques for overcoming high noise levels which are invariably present in thermal data. Vavilov, Grinzanto et al's normalized contrast (time domain) technique[1] and Maldague, Marinetti et al's pulse phase (frequency domain) technique [2,3] mark two major trends in this direction, each with its own claim of wide ranging applicability.

The present paper aims at making a critical comparison of the above two techniques, by applying them on an experimental situation where non-uniformity of the heat source and anisotropy of material thermal properties combine to create a typical adverse situation for thermographic NDT. Pulse thermography carried out with a conventional heat source, which invariably had a non-uniform radiation profile, a simple easy-to-use fixture, which further added to this non-uniformity and an anisotropic cfrp laminate, having rayon-based carbon fabric as reinforcement with porous phenolic resin as matrix, had been used for creating this truly adverse experimental situation.

Finally, an attempt has been made in this paper to assess the capability of each of these data analysis techniques for detection of defects embedded at different depths of the cfrp laminate, to weigh the pros and cons and then to chalk out a logical route for reliable defect detection in composites.

2.0 THEORETICAL BACKGROUND

Output temperature signal generated by a thermography system interrogating a test object is generally corrupted by various types of noise [1] as represented by the following equation

$$U(x,y,\tau) = E(x,y,\tau) \quad T_u(\tau,L,D,Q) + A(x,y,\tau) + N_d$$

$U(x,y,\tau)$=output signal corresponding to (x,y) spatial coordinates at time τ

E=structural noise due to fluctuation in absorbency and emissivity of the material under test

$T_u(\tau,L,D,Q)$=corresponding uncorrupted time signal, which is a function of τ (time),

L(specimen thermal properties), D(location, lateral size and depth of defect) and Q(heat source characteristics)

$A(x,y,\tau)$=additive white noise due to radiation reflected from the surface of the test object

N_d=white noise generated by the IR detector

Extracting the uncorrupted surface temperature profile by eliminating various types of noise from the recorded signal is therefore of crucial importance in thermographic NDT.

In order to tackle this problem, Vavilov et al [1,5] had proposed using a derived parameter called normalized contrast for imaging as explained below.

If the recorded temperature signal over a defect is

$$\Delta T(x, y, \tau) = T(x, y, \tau) - T(x_{ref}, y_{ref}, \tau)$$

where x,y and x_{ref}, y_{ref} refer to the spatial co-ordinates of two points selected in defect zone and defect free zone (but close to the defect zone) respectively, then the corresponding normalized contrast is defined as

$$C^{norm}(x, y, \tau) = \frac{T(x, y, \tau)}{T(x, y, \tau_{norm})} - \frac{T_{ref}(x, y, \tau)}{T_{ref}(x, y, \tau_{norm})}$$

where τ_{norm} is a particular time frame whose corresponding temperature values with respect to different pixels are used for normalization of corresponding pixel values in all other frames. Vavilov had used maximum temperature at the end of heating as the normalizing frame, applicability of which under different heating regimes needs to be ascertained. It is important to note here that in addition to choice of normalizing time frame, apriori knowledge of a non-defect zone (located close to the defect) demands extremely high level of skill and experience on the part of the operator, which is not always available.

An alternative method of data analysis by pulsed phase imaging has been proposed recently by Maldague et al [2,3,4]. The heating pulse in pulsed thermography can be represented as a combination of sinusoids, by taking Fourier transforms. During cooling cycle the surface temperature transients are recorded as in standard pulse-thermography and Temp-time curves are plotted corresponding to each pixel. Next Fourier transform of each such T-t profile is computed and the phase corresponding to each frequency is determined from the relation

$$\Phi(\omega) = \tan^{-1} \frac{I(\omega)}{R(\omega)}$$

where $\phi(\omega)$=phase at frequency ω and $I(\omega)$, $R(\omega)$ are imaginary and real parts of the Fourier transform at frequency ω. The phase image can be plotted by making phase at a particular frequency represent the corresponding pixel value. Therefore phase difference $\delta\phi$ between a defect point and a reference point makes the defect visible in the phase image.

Advantage of this procedure lies in the fact that a phase image, which is related to propagation time delays, should be independent of optical and infra-red surface features and therefore should show improved quality. An attempt has been made in this paper to try out both normalization and phase image concepts mentioned above for evaluating defects in CFRP.

3.0 EXPERIMENTAL SET-UP AND PROCEDURE

The work was carried out with an agema thermovision 870 camera with thermoelectrically cooled SPRITE detectors. The spectral response was in 2-5μm range. A CFRP laminate with tailored defects was heated by a 1000W commercial halogen lamp with an effective heating area of 220 X 135 mm^2 for a specific time interval 't'. Following this thermograms were captured from the same side at 6Hz sampling frequency for every pixel, till thermal equilibrium was attained.

3.1 LAMINATE WITH TAILOR MADE DEFECTS

A 300mm X 300mm X 2mm cfrp laminate with 5 layers of carbon-fabric impregnated with phenolic resin, each of approximately 0.4mm thickness was made using a metallic mould and cured in a hydraulic press. Four Teflon inserts each of 10mm dia and 0.1mm thickness was placed at four different layers of the laminate (i.e.

at depths of 0.4mm, 0.8mm, 1.2mm, 1.6mm) to create typical defects as shown in fig.1

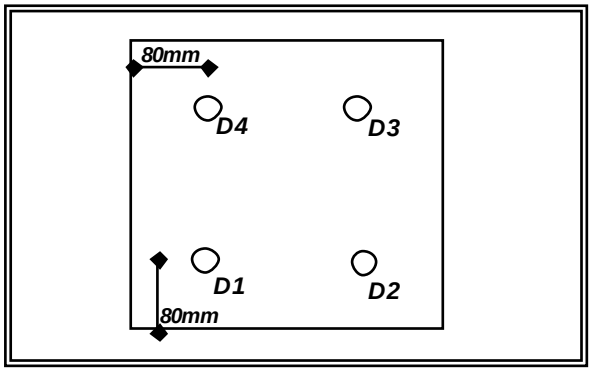

Fig.1 Configuration of the 10mm dia defects in laminate with the following depths; D1-0.4mm, D2-0.8mm, D3-1.2mm, D4-1.6mm

The defect area of interest in the laminate was heated using the halogen lamp for 10 seconds, subsequently it was switched off and removed. The IR camera was then used to capture the surface temperature profile during the cooling down phase, frame by frame at the rate of 6 Hz per pixel, till near equilibrium with the surroundings was reached. A schematic diagram of the test configuration is presented in fig 2.

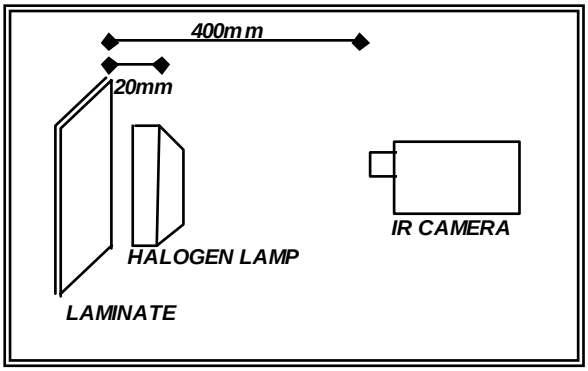

Fig.2 Test configuration for Laminate

4.0 RESULTS AND DISCUSSIONS

Thermal data acquired during the cooling phase of each defect was subjected to two different types of analysis, as stated below: Normalised temperature image using time domain data; Phase image corresponding to selected band of frequency, using frequency domain representation.

The procedures and the results pertaining to above modes of analysis are presented below.

4.1 NORMALISED TEMPERATURE IMAGES: TIME DOMAIN ANALYSIS

Typical maximum temperature images corresponding to defects D1, D2, D3 and D4 captured immediately after switching off of the lamp, are shown in figs. 3,6,9 and 12 respectively. Time temperature profiles corresponding to typical selected pixels (eg. at defect, far from defect, at non-defect hot spot etc.) of D1, D2, D3, D4 cases are presented in figs. 5,8,11,14 respectively, where the follower designations (a) and (b) of each of these figures signify a particular T-t profile before and after normalization (w.r.t. the first frame at t=0) respectively.

The best normalized images (corresponding to the most favourable times selected from the T-t profiles) are presented for the defects D1, D2, D3 and D4 in figs. 4, 7, 10 and 13 respectively. The salient features of figs. 3 to 14 are summarized below:

(i) The raw images of D1 and D2 (figs. 3 & 6) show expected high temp defect zones, together with undesirable hot spots in non-defect zones, which makes reliable detection of defects problematic. However, normalization in these two cases could very effectively overcome the above problem, as is evident from clear definition of normalized images 4 & 6 for defects D1 and D2 respectively. This was due to the fact that the defect zone cooled faster than its immediate surroundings.

(ii) However it may be noted that same was not the case for D3 defect. Here due to larger defect depth, appreciable rise of temperature was not observed in the defect zone, as compared to its surroundings (ref. raw images of D3 in fig.9), thereby making defect indication in the raw image impossible. To make the situation even worse, the T-t profiles of defect and non-defect zones run parallel to each other in this case, as is evident from the normalized T-t plot of fig.11.b and also from complete loss of defect contrast in the normalized thermogram of fig.10.

(iii) In case of defect D4, temperature rise above the defect was not appreciable due to larger depth of the defect. Because of this, the defect was not detectable as a hot spot in the maximum

temperature raw image. (ref. fig 12) However, the normalized T-t plots of fig 14.b clearly indicate faster cooling rate of the defect zone, as against its surroundings. Consequently in some later frames of the captured image, the defect D4 stands out as a cold spot with reasonable clarity (ref. fig. 13). Inspite of this, it is still quite possible to miss this defect D4, because the required contrast is restricted here only within a few frames.

It may be mentioned here that complete disappearance of defect observed in the normalized image of the defect D3 in fig.10 is caused by a special combination of non-uniform heating effect, diffusivity difference between teflon and cfrp and anisotropy of heat conduction in thickness and in lateral directions. In a more frequently occurring situation, the D3 case is very similar to the D4 case, where limited defect contrast is achievable only in certain frames. An example of this has been included later in fig.16.a.

4.2 PHASE IMAGES: FREQUENCY DOMAIN ANALYSIS

The experimental T-t profiles were represented in frequency domain by Fourier transforms. From the real and imaginary parts of DFT, the phase value (ϕ) corresponding to each pixel was calculated. Difference ($\Delta\phi$) between the phase value of the particular pixel and the phase value of a known defect-free pixel was finally used as the informative parameter for plotting the phase image. Special care was taken towards avoiding possible errors due to aliasing and low frequency resolution, as explained below.

Within the limits of the available hardware, the experimental data could be captured only at the rate of 6Hz per pixel upto a record length of n=406. In addition to this, equilibrium temperature attained at a particular instant of time was also recorded. The experimental T-t data (406) was extrapolated to 8000 data points (at 6Hz sampling frequency) using a fourth order polynomial fit. Subsequently, the sampling frequency was artificially increased four-fold, using cubic spline interpolation. Thus by a combination of extrapolation and interpolation, the frequency range and the frequency resolution of the Fourier transform could be effectively enhanced from 0-3Hz to 0-24Hz and from 0.0148 Hz to 0.00075 Hz respectively. The phase difference data calculated from the above Fourier transforms were suitably sliced at particular frequency bands, in order to generate the required phase images. Typical $\Delta\phi$ images (frequency selected) for defects D2, D3 and D4 are shown in figs. 15.b, 16.b and 17.b respectively. Corresponding highest contrast normalized images generated using the same data set are included in figs. 15.a, 16.a and 17.a respectively for comparison.

It is observed that, (i) In case of D2 defect both normalized image and phase image give excellent results. The same was also observed in D1 case, as is expected; (ii) In case of D3 and D4 defects located at larger depths, the frequency selected $\Delta\phi$ image had revealed the defect with improved contrast. Certain non-uniformities in the quality of the cfrp laminate could also be revealed in the $\Delta\phi$ image. The horizontal patch running across the D4 image (ref. Fig.17.b) is an example of such variation in the quality of the laminate, which could not be revealed by the normalized image (ref. Fig.17.a). However, keeping in view the difficulties of conducting reliable thermography inspection in a truly adverse situation (comprising of deeper defects, non-uniformity of heat source and extremely high lateral conduction effect of rayon-based carbon-fabric impregnated with a high porosity resin matrix) it seems advisable to look at both normalized time domain images and frequency selected $\Delta\phi$ images for improving probability of defect detection and also for minimizing the probability of false alarm.

In a material with high thermal anisotropy like the present cfrp laminate, a thermal pulse propagated through distance 'd' in lateral direction is expected to be richer in high frequency components than the same pulse propagated to depth 'd' in thickness wise direction. Due to such anisotropy of spectral content of propagating pulses, frequency slicing of $\Delta\phi$ image appears to offer much promise for NDE of anisotropic materials by thermography.

This point needs further investigation based on a wider range of defect and material data.

5.0 CONCLUSION

i. Tailor-made defects generated in a cfrp laminate with high anisotropicity have been investigated by thermography using a conventional heat source and 6Hz per pixel IR Camera.

ii. The normalized images have successfully revealed the shallow defects. Detection of deeper defects by this technique has been extremely problematic, ranging between bare visibility to complete loss of defect contrast.

iii. By a judicious combination of interpolation and extrapolation techniques and its frequency domain analysis, it has been possible to achieve reasonable defect contrast in the frequency selected phase ($\Delta\phi$) images in all cases.

iv. It is finally being concluded that at least for deeper defects embedded in a highly anisotropic material, both normalized time domain images and frequency selected $\Delta\phi$ images should be generated and cross-checked, for maximizing the probability of defect detection and also for minimizing the probability of false alarm.

6.0 REFERENCES

1. Vladimir P.Vavilov, Ermanno Grinzato, Paolo G.Bison, Sergio Marinetti and Chiara Bressan, 'Thermal Characterization and Tomography of Carbon Fiber Reinforced Plastics using Individual Identification Technique', *Materials Evaluation* (May 1996), p.604
2. X.Maldague, S.Marinetti, 'Pulse Phase Infrared Thermography', *Journal of Applied Physics* 79[5]: 2694-2698 (1996)
3. X.Maldague, S.Marinetti, J.P.Couturier, 'Applications of Pulse Phase Thermography', *Review of Progress in Nondestructive Evaluation*, Vol.16(1997), p.339
4. Xavier P.V. Maldague, 'Non-destructive evaluation of materials by infrared thermography', Springer Verlag (1992)
5. V.Vavilov, X.Maldague, B.Dufort, F.Robitaille and J.Picard, 'Thermal non-destructive testing of carbon-epoxy composites – detailed analysis and data processing', *NDT&E International* Vol.26. No.2(1993) p.85

FIG.3
MAXIMUM TEMPERATURE THERMOGRAM OF D1

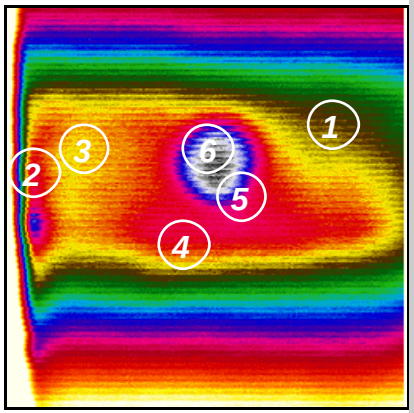

FIG.4
ONE OF THE NORMALIZED IMAGES OF D1

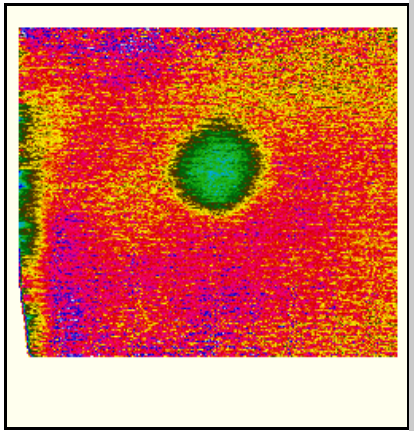

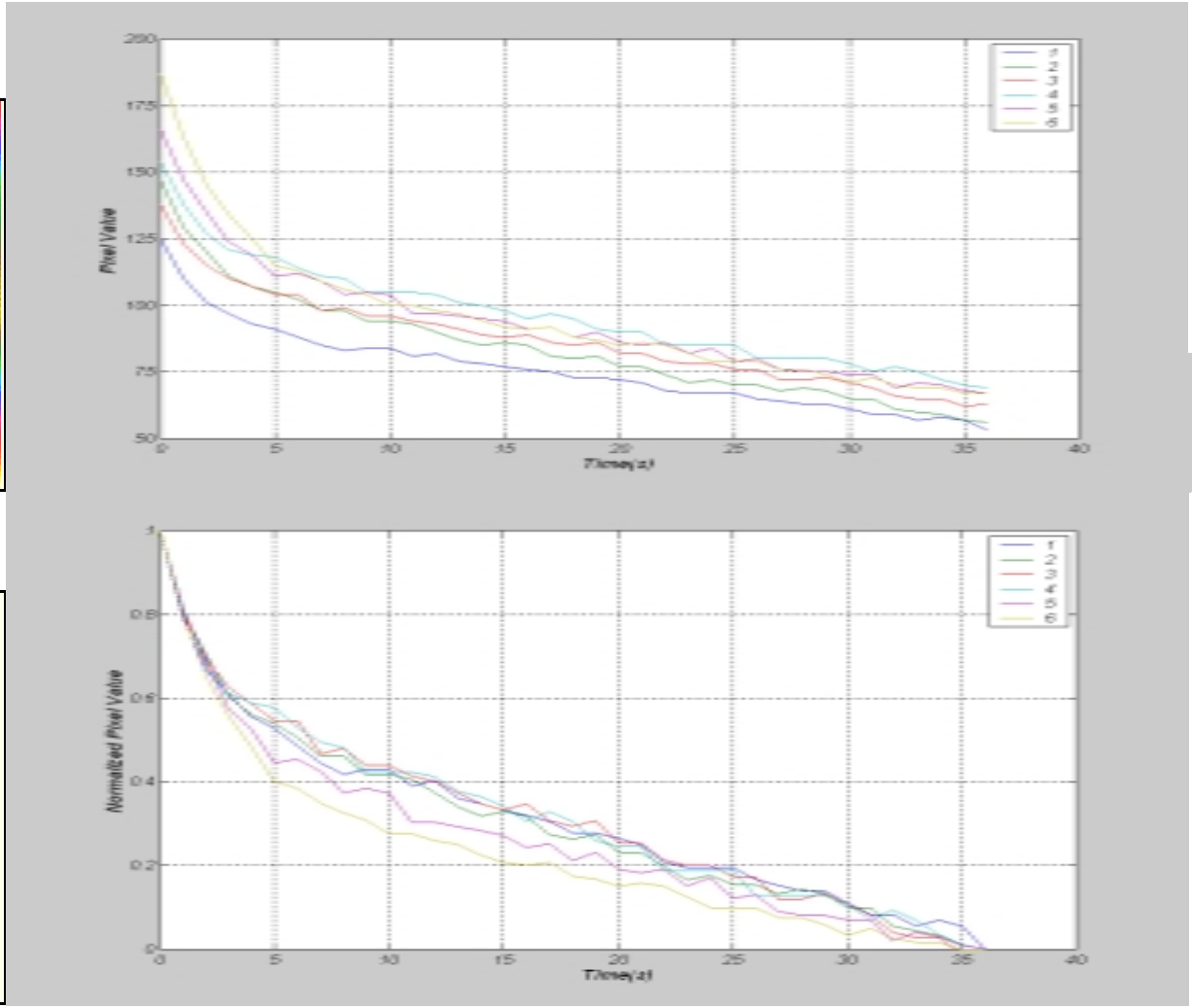

FIG.5.A
TEMPERATURE-TIME PROFILES AT 6 DIFFERENT POINTS ON THE THERMOGRAM

FIG.5.B
NORMALIZED TEMPERATURE-TIME PROFILES AT 6 DIFFERENT POINTS ON THE THERMOGR

FIG.6
MAXIMUM TEMPERATURE THERMOGRAM OF D2

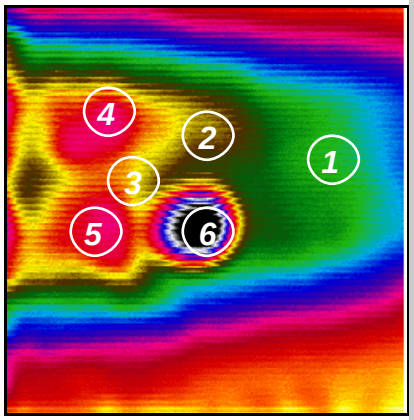

FIG.7
ONE OF THE NORMALIZED THERMOGRAMS OF D2

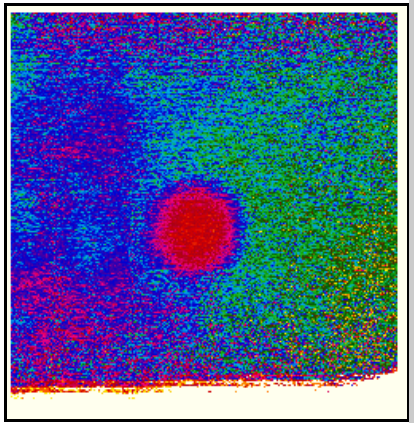

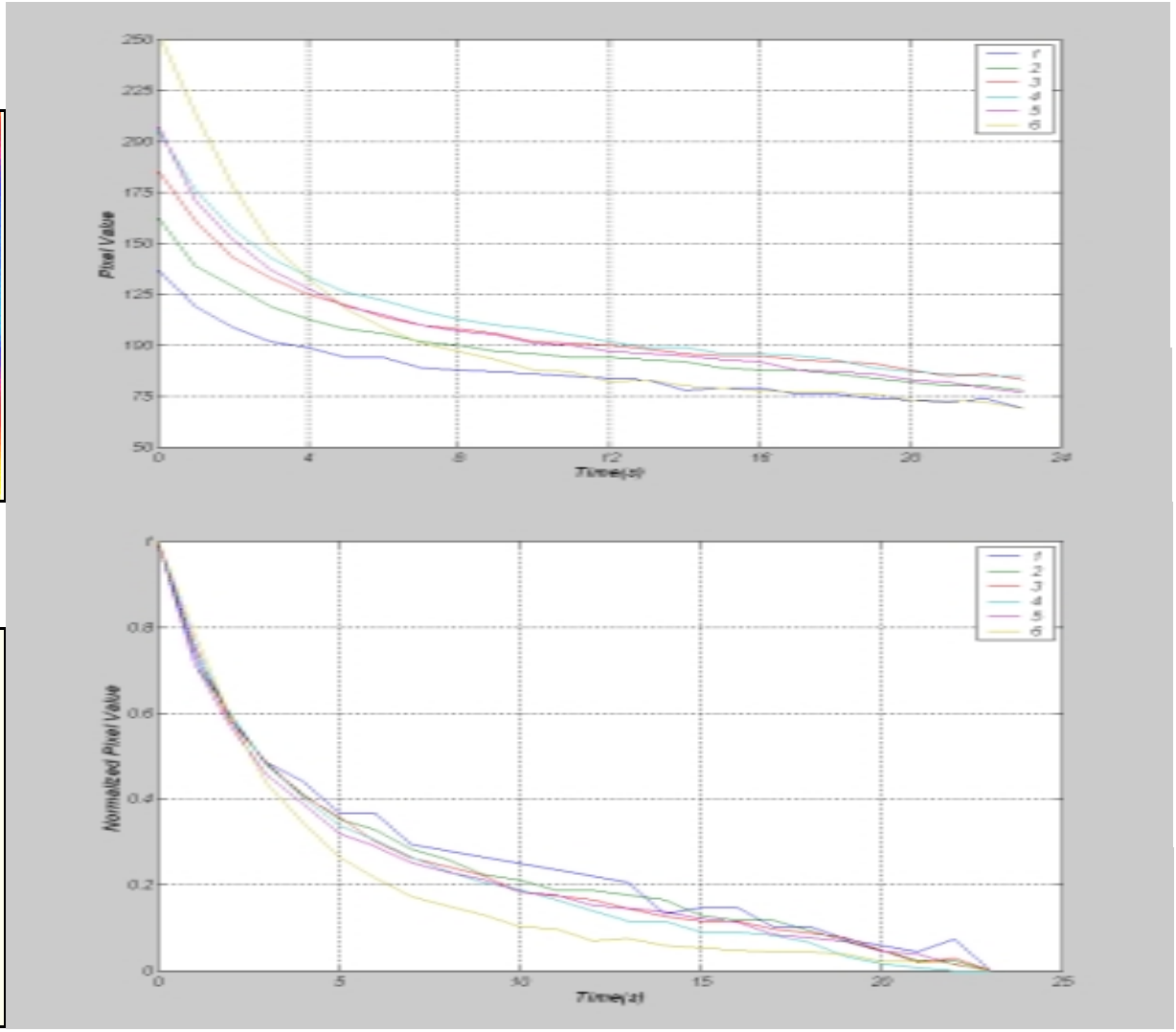

FIG.8.A
TEMPERATURE-TIME PROFILES AT 6 DIFFERENT POINTS ON THE THERMOGRAM

FIG.8.B
NORMALIZED TEMPERATURE-TIME PROFILES AT 6 DIFFERENT POINTS ON THE THERMOGR

FIG.9
MAXIMUM TEMPERATURE THERMOGRAM OF D3

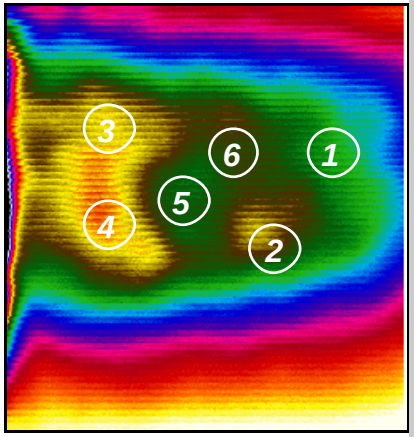

FIG.10
ONE OF THE NORMALIZED THERMOGRAMS OF D3

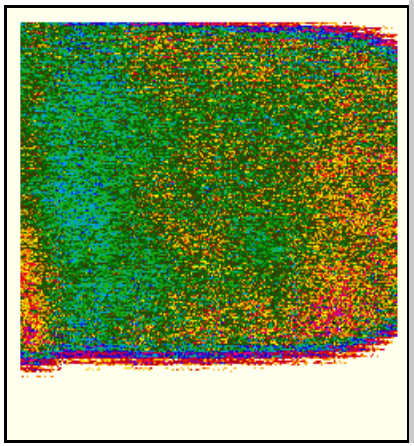

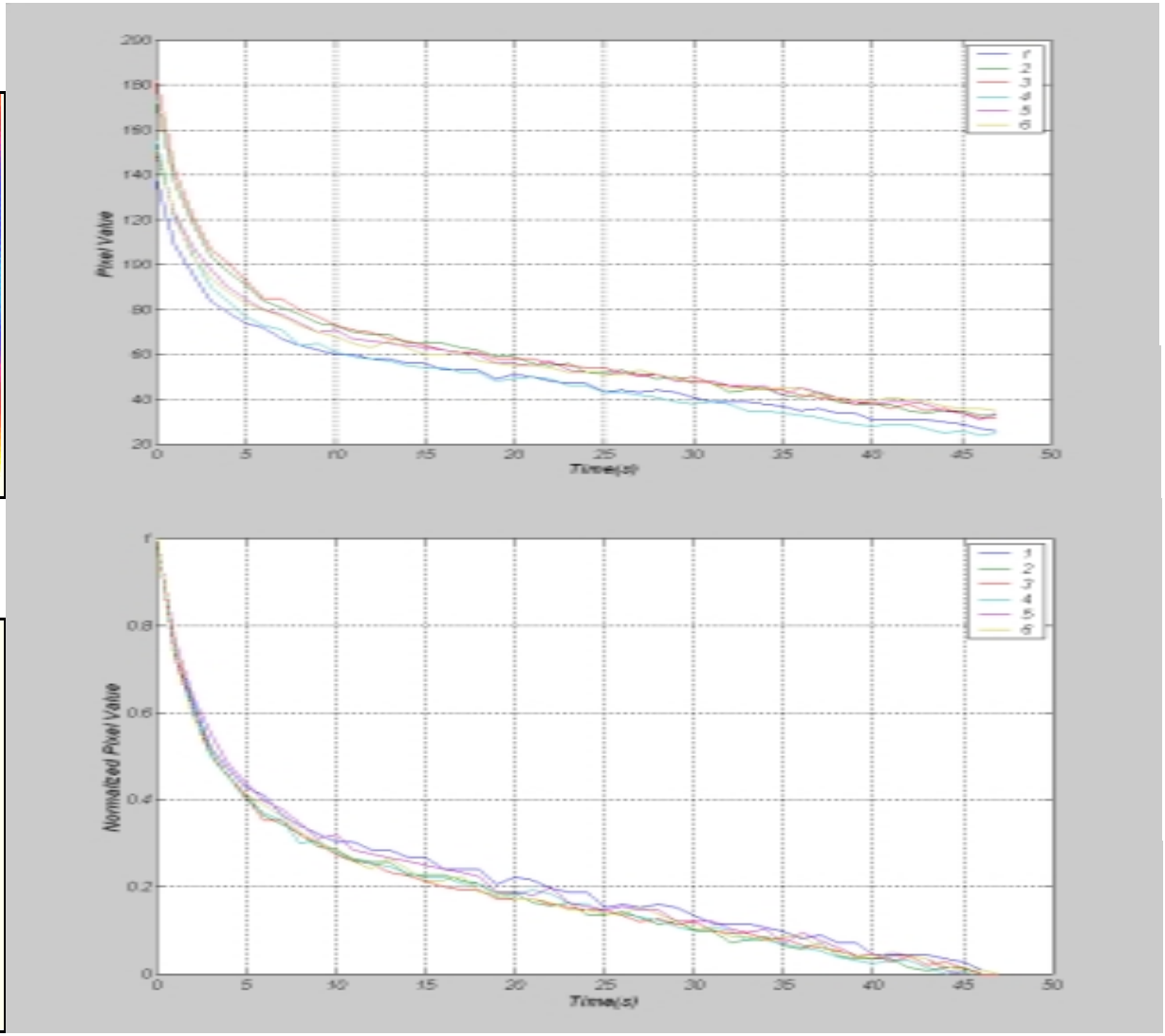

FIG.11.A
TEMPERATURE-TIME PROFILES AT 6 DIFFERENT POINTS ON THE THERMOGRAM

FIG.11.B
NORMALIZED TEMPERATURE-TIME PROFILES AT 6 DIFFERENT POINTS ON THE THERMOGR

FIG.12
MAXIMUM TEMPERATURE THERMOGRAM OF D4

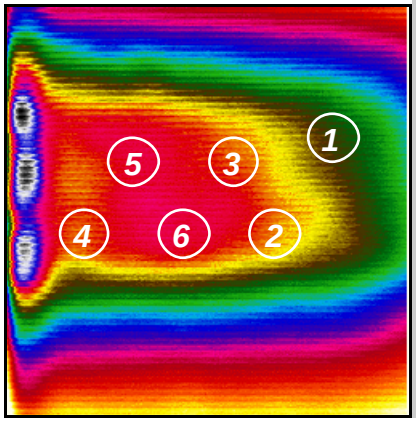

FIG.13
ONE OF THE NORMALIZED THERMOGRAMS OF D4

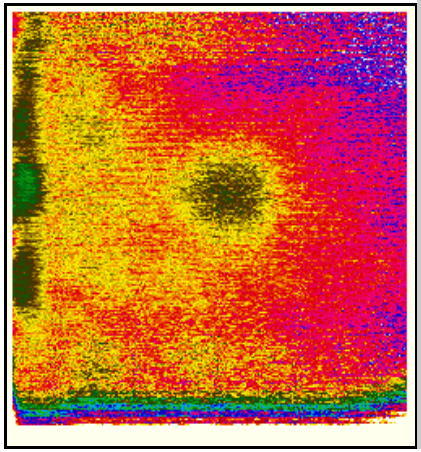

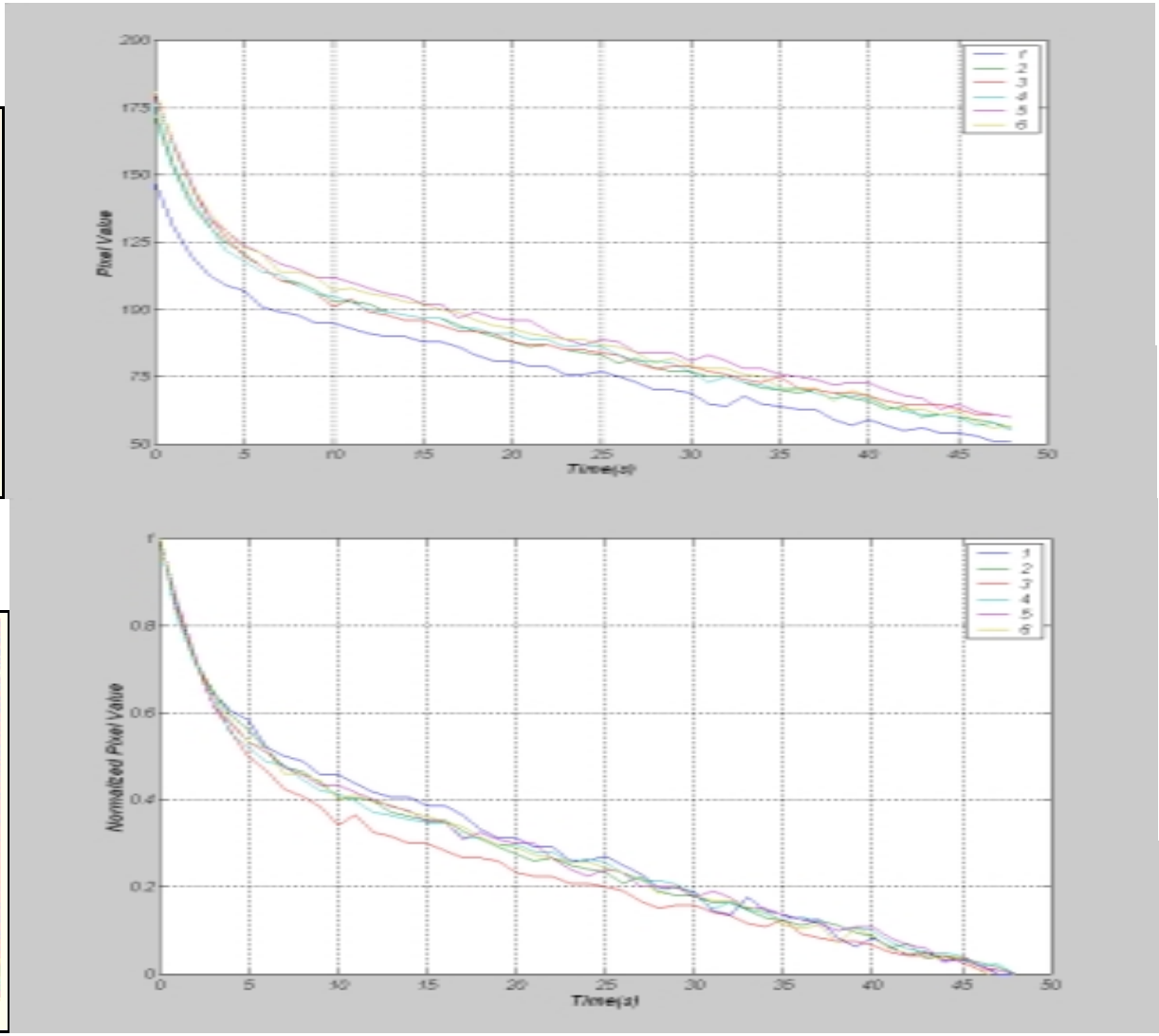

FIG.14.A
TEMPERATURE-TIME PROFILES AT 6 DIFFERENT POINTS ON THE THERMOGRAM

FIG.14.B
NORMALIZED TEMPERATURE-TIME PROFILES AT 6 DIFFERENT POINTS ON THE THERMOGR

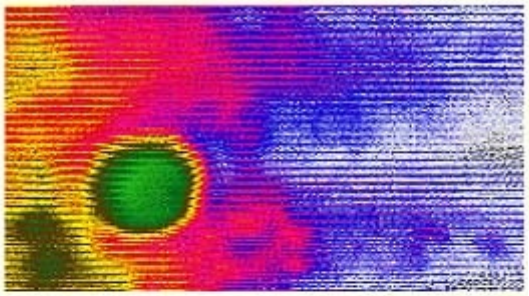

Fig. 15(a)
D2 on normalisation

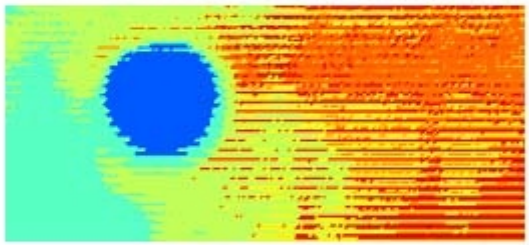

Fig. 15(b)
D2 on phase imaging
between 0.045Hz to 0.0525Hz

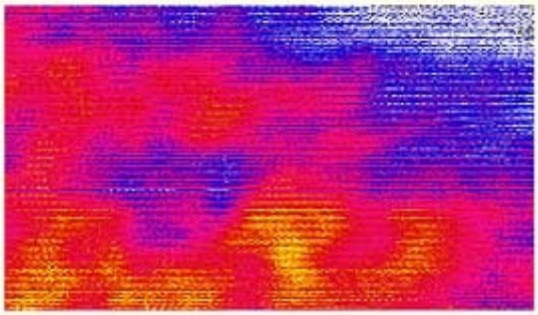

Fig. 16(a)
D3 on normalisation

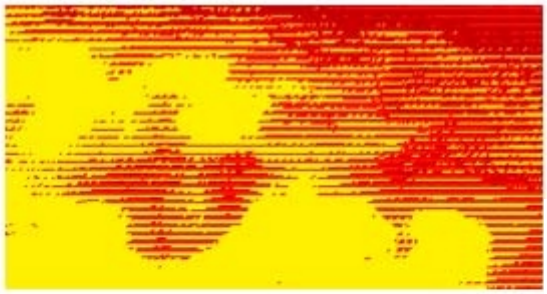

Fig. 16(b)
D3 on phase imaging
between 0.03Hz to 0.0375Hz

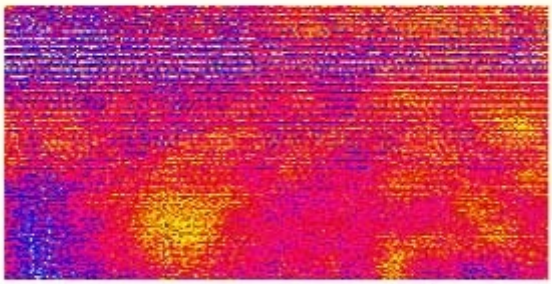

Fig. 17(a)
D4 on normalisation

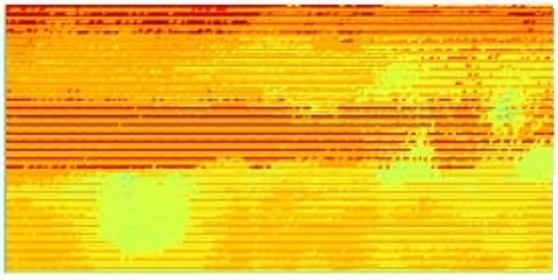

Fig. 17(b)
D4 on phase imaging
between 0.03Hz to 0.0375Hz